NANO LETTERS

2009
Vol. 9, No. 6
2367-2371

# Alternating Current Driven Electroluminescence from ZnSe/ZnS:Mn/ZnS Nanocrystals

**Vanessa Wood,[†,‡] Jonathan E. Halpert,[†,§] Matthew J. Panzer,[‡] Moungi G. Bawendi,[§] and Vladimir Bulović*[,‡]**

*Department of Electrical Engineering and Computer Science and Department of Chemistry, Massachusetts Institute of Technology, Cambridge, Massachusetts 02139*

*Received March 20, 2009; Revised Manuscript Received April 17, 2009*



## ABSTRACT

**We present a novel technique for room temperature, solution-based fabrication of alternating current thin-film electroluminescent (AC-TFEL) devices using phosphor-doped nanocrystals. Synthesis for stable ZnSe/ZnS:Mn/ZnS nanocrystals that exhibit a quantum yield of 65 ± 5% is outlined, and their electroluminescence is demonstrated in structures consisting of only wide band gap ceramic layers. Both the nanocrystal and the ceramic films have minimal absorption across the visible light spectrum, enabling us to demonstrate transparent AC-TFEL devices.**

Alternating current thin-film electroluminescent (AC-TFEL) devices already occupy a segment of the large area, high-resolution, flat panel display market. AC-TFEL displays are robust, possess long lifetimes, and offer high luminance with relatively low power consumption.[1] AC-TFEL devices consist of a phosphor layer, such as manganese-doped zinc sulfide (ZnS:Mn), vertically sandwiched between two insulators that are contacted by electrodes. When a sufficiently high voltage is applied across the electrodes, electrons trapped at interfaces between the layers are injected into the conduction band of the phosphor, where they are accelerated by the field and can excite the luminescent dopant centers in the phosphor layer via impact excitation and ionization mechanisms.[2,3]

While fabrication of AC-TFEL devices have been the subject of considerable study over the past 3 decades, challenges remain. Development of multicolor displays with balanced red, green, and blue (RGB) emission has proven difficult as the most efficient red, green, and blue phosphors comprise different materials systems that require different deposition and annealing steps.[1,4,5] Additionally, differences in luminous efficiencies of different colors can span an order of magnitude, complicating electronic driving of balanced color displays.[1,4,5] Transparent AC-TFEL displays have recently been demonstrated by Sharp, Inc.; however, the processing of the phosphor to achieve transparency is difficult and has not yet been developed for phosphors other than ZnS:Mn.[6]

In this Letter, we present a novel materials system for the active phosphor layer in transparent AC-TFEL devices. We use colloidally synthesized Mn-doped nanocrystals to demonstrate electroluminescence (EL) from a solution-deposited active layer in an AC-TFEL device fabricated at room temperature. Wide band gap host nanocrystals and wide band gap metal oxides enable transparent device structures without additional processing steps beyond the room-temperature layer-by-layer deposition of each material set.

To date, colloidal nanocrystals have successfully been doped with transition metals (such as Fe, Ni, Mn, Cu) and lanthanides (such as Eu, Er, Tm, Tb) to alter their electronic, optical, or magnetic properties.[7−12] If the excitation energy of the dopant is smaller than the band gap of the host material, the photoluminescence of the doped nanocrystal is determined by the dopant atoms; light emission is independent of the band gap of the host material and largely immune to thermal and chemical variations of the surrounding medium.[13] For example, by using different dopants or various synthetic procedures,[14] the emission wavelength of doped ZnSe nanocrystals can be tuned from the blue through the red, suggesting the possibility of developing multicolored AC-TFEL displays. However, until now, there has been no demonstration of EL from phosphor impurity dopants in ZnSe or other wide band gap host nanocrystals. Luminescence of CdS:Mn/ZnS nanocrystals embedded into a polymer-LED was observed;[15] however, color-tunable doping or a transparent device is challenging to achieve with this structure because of the relatively small band gap of CdS. In order for these doped nanocrystals to be luminescent at the colors of the dopant, the excitation energy of the dopant

* Corresponding author, bulovic@mit.edu.
† These authors contributed equally to this work.
‡ Department of Electrical Engineering and Computer Science.
§ Department of Chemistry.

10.1021/nl900898t CCC: $40.75 
**Published on Web 04/27/2009**

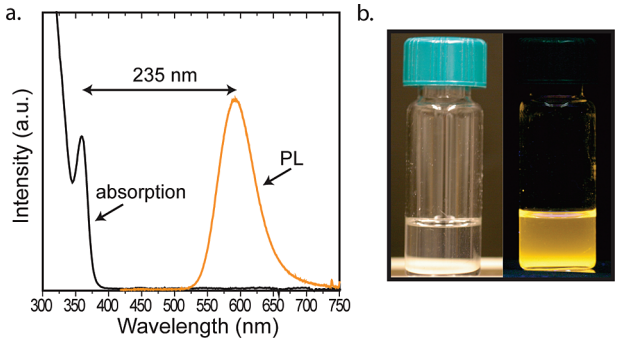


**Figure 1.** (a) The absorption (black line) and photoluminescence (orange line) spectra of the ZnSe/ZnS:Mn/ZnS nanocrystals in solution show a large (235 nm) Stokes shift. (b) Photographs of a vial of ZnSe/ZnS:Mn/ZnS nanocrystals in chloroform under room lighting (left) and under UV illumination (right) provide visual confirmation of the spectra shown in panel a, which indicate that these orange-emitting nanocrystals exhibit no absorption in the visible wavelength regime.

needs to be smaller than the band gap of the host material to enable energy transfer of an exciton on the nanocrystal core to the impurity dopant. Furthermore, when the nanocrystal host material is a wide band gap semiconductor such as ZnSe, thin films of nanocrystals do not absorb in the visible wavelength region (see Figure 1a), making them compatible with the construction of transparent devices. Such devices could be used for displays with two-way, heads-up viewing capabilities.

Colloidal solutions of doped nanocrystals also bring a key advantage to the fabrication of AC-TFEL displays. Solution processing of nanocrystalline colloids enables a wide range of deposition techniques such as spin-casting,[16,17] microcontact printing,[18] inkjet printing,[19] and electrospray[20] to be employed for their integration into electroluminescent devices. Previously, some of these printing techniques have been used to demonstrate side-by-side patterning of nanocrystals of different emission colors with up to 1000 dpi pattern resolution (25 $\mu$m features), as would be necessary for high-resolution displays.[18] In our demonstration of the transparent AC-TFEL device we use multilayer spin-casting of phosphor-doped nanocrystal solutions for the active emissive layer.

We choose to work with Mn-doped nanocrystals as Mn is the most commonly used phosphor dopant in AC-TFEL devices. We report a synthesis of ZnSe/ZnS:Mn/ZnS nanocrystals that offers the stability and high quantum yield needed for AC-TFEL applications. The high quantum yield of these ZnSe/ZnS:Mn/ZnS nanocrystals is due to their thick ZnS shell, which localizes the excited state on the Mn-dopant atom by preventing energy transfer to surface states or the surrounding medium. The thick shell also improves the stability of the nanocrystal, preventing migration of the Mn dopant.

The synthesis of ZnSe/ZnS:Mn/ZnS nanocrystals used in this study is adapted from Thakar et al.[21] The ratio of Zn and S precursors in the overcoating step, the final ZnS shell thickness, and the ligand chemistry possible account for the greater quantum yield in our nanocrystals. ZnSe cores are prepared by injecting 96 mg of diethyl zinc and 0.67 mL of trioctylphosphine (TOP) selenide into a flask of 10 mL of oleylamine, degassed at 140 °C. After the mixture was heated at 270 °C for 90 min, the flask is cooled to 170 °C and a solution of 45 mg of manganese stearate, 76 mg of diethyl zinc, and 160 mg of hexamethyldisilathiane in 6 mL of TOP is added at a rate of 1 drop/s. These ZnSe/ZnS:Mn particles are precipitated twice using methanol and butanol and redispersed in hexane. This solution is then added to a degassed flask containing 10 g of trioctylphosphine oxide (TOPO) and 0.4 g of *n*-hexylphosphonic acid (HPA) at 80 °C. The hexane is removed under vacuum. The flask is then placed under argon and heated to 170 °C. A solution of 80 mg of diethyl zinc and 160 mg of hexamethyldisilathiane in 5 mL of TOP is added dropwise, and the flask is cooled to room temperature. Four milliliters of hexane and 4 mL of butanol are then added. The ZnSe/ZnS:Mn/ZnS nanocrystals are finally precipitated twice using methanol and butanol and redispersed in chloroform.

Figure 1a shows the absorption and photoluminescence (PL) spectra for these nanocrystals in solution. As discussed previously, the nanocrystals do not absorb in the visible wavelength region because the host material, ZnSe, is a wide band gap semiconductor. The PL spectrum is centered at wavelength $\lambda = 590$ nm, which is characteristic of the Mn $^4T_1 \rightarrow {}^6A_1$ phosphor transition.[21] Streak camera measurements of this luminescence reveal an excited state lifetime in excess of 1 ms, consistent with the expected phosphorescent emission decay mechanism. The photographs of the nanocrystals in room light and under UV illumination (Figure 1b) provide a visual indication of the transparency of the nanocrystals as well as their high quantum yield (QY), which we measure to be 65 ± 5% for the nanocrystals in solution. A direct measurement of QY by comparing the solution to an organic dye is not possible due to the large Stokes shift in the ZnSe/ZnS:Mn/ZnS nanocrystals. The QY measurement is therefore performed by comparing the nanocrystal solution to a solution of orange emitting CdSe/ZnS quantum dots with a QY of 65%, previously calibrated to a solution of Rhodamine 610 (QY = 95%). In addition to having a high QY, the ZnSe/ZnS:Mn/ZnS nanocrystal solution also exhibits a long shelf life. Figure 1b shows a nanocrystal solution synthesized over 1 year prior to the date of the photographs.

The AC-TFEL device structure that enables electrical excitation of the doped nanocrystals is shown schematically in Figure 2a. It is fabricated using room temperature radio frequency (rf) magnetron sputtered ceramics and solution-deposited nanocrystals. We begin by sputtering 80 nm of an insulating metal oxide of either $Al_2O_3$ or $HfO_2$ onto commercially deposited indium tin oxide (ITO) on glass from Thin Film Devices, Inc. Both the bottom and top insulating layers are sputtered in an inert Ar environment at 4 mTorr with a power of either 150 W (for $Al_2O_3$) or 100 W (for $HfO_2$). The sputter-deposited insulating films are complete and planar, as revealed by atomic force microscopy (AFM) characterization. For a device consisting of $Al_2O_3$ layers, for example, we measure a root-mean-square (rms) surface roughness of 0.3 nm for the bottom layer and a surface

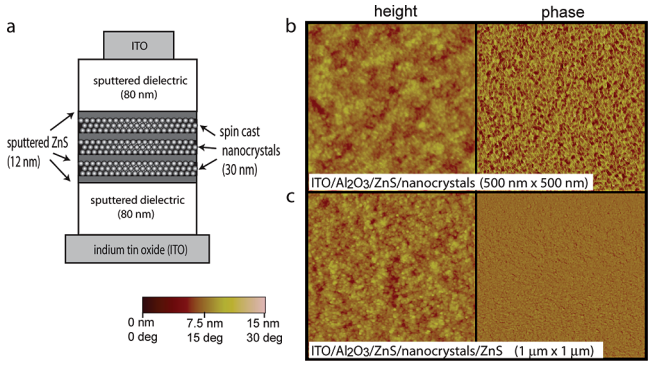


**Figure 2.** (a) A schematic of the doped nanocrystal-based AC-TFEL device structure. AFM topographic and phase images show (b) the first layer of nanocrystals spin-cast on ZnS and (c) a subsequent layer of ZnS sputtered on top of the nanocrystals. Comparison of the phase images in panels b and c shows that the nanocrystals are completely covered by the 12 nm layer of ZnS.

roughness of 0.9 nm (rms) for the top layer. The observation of sub-1-nm roughness over a 5 $\mu$m $\times$ 5 $\mu$m area of the top insulating layers indicates that the multiple ZnS and nanocrystal layers in the middle of the device structure maintain planarity throughout the multilayer growth.

The active layer of the device consists of alternating layers of sputtered ZnS and spin-cast ZnSe/ZnS:Mn/ZnS nanocrystals. Each layer of ZnS is 12 nm thick and is sputter-deposited with a power of 25 W in 4 mTorr of Ar. A thickness of 12 nm of ZnS is chosen because it is enough to form a complete layer that is not damaged upon subsequent spin-casting of the next nanocrystal layer. Thicker ZnS layers, while also complete and capable of withstanding the subsequent spin-casting steps, increase the turn on voltage of the device. The layers of nanocrystals are spin-cast in a nitrogen glovebox onto the ZnS at a speed of 1200 rpm from chloroform. Cross sectional AFM scans indicate that the total thickness of each layer of nanocrystals is approximately 30 nm, corresponding to approximately four to five layers of nanocrystals. Panels b and c of Figure 2 show AFM topography and phase images of the nanocrystal layer and the first ZnS layer on top of the nanocrystals. Figure 2b reveals a highly monodisperse film of 5 nm diameter nanocrystals. The rms roughnesses of the two layers are 1 and 0.8 nm, respectively, indicating that both the nanocrystals and the ZnS form smooth, complete layers. The contrast between the phase images in panels b and c of Figure 2 (right-hand panel) further confirms the completeness of the ZnS layer on top of the nanocrystals. The device is completed with a second, 80 nm thick insulating layer and a 150 nm thick top electrode of either ITO or Al, which are sputtered at 35 W in 4 mTorr of Ar. Use of top ITO electrodes results in a highly transparent completed structure.

In the AC-TFEL architecture presented here, the alternating layers of ZnS and nanocrystals are necessary for device electroluminescence (EL). To confirm that the ZnS layers are critical to device operation, we fabricate four devices with continuous 30 or 90 nm thick layers of ZnSe/ZnS:Mn/ZnS nanocrystals sandwiched between both $Al_2O_3$ and $HfO_2$ dielectric layers. The 90 nm thick layer is spin-cast using a more concentrated solution of nanocrystals, and its thickness and uniformity are characterized by AFM, as described previously. No EL is observed from these devices, indicating that the device luminescence is determined by the number of ZnS layer−nanocrystal interfaces and not by the number of luminescent impurity centers.

To determine the optimal number of ZnS layers within the device, we fabricate structures with two, three, four, or five 12 nm thick ZnS layers (sandwiching one, two, three, or four layers of nanocrystals, each of which is 30 nm thick). Eighty nanometer thick $Al_2O_3$ layers are used as the dielectrics for the four devices with Al as the top contact. EL is measured while the devices are biased with a square-wave pulse at a frequency of 30 kHz and peak-to-peak voltage ($V_{pp}$) of 110 V. The trend in EL response is shown in Figure 3a. The luminescence from the device with two layers of ZnS is below our reliable detection threshold. We find four layers of ZnS to be optimal; devices with three and five layers of ZnS (containing two or four layers of nanocrystals, respectively) exhibit lower EL intensity than the device with four ZnS layers. The device with five layers of ZnS (and four layers of nanocrystals) can operate at the same brightness as the four ZnS layer device but requires an increased operating voltage to do so because of the additional voltage drop across the insulating layers of ZnS and nanocrystals. Likewise, devices with multiple 90 nm thick nanocrystal layers exhibit electroluminescence but require higher operating voltages than devices with 30 nm thick nanocrystal layers to achieve the same field drop across the nanocrystal layers. These results demonstrate the importance of maximizing both the number of interfaces and the electric field dropped across the nanocrystal layers.

The following results pertain to transparent devices with four layers of ZnS and three 30 nm thick layers of nanocrystals, depicted schematically in Figure 2a. The photographs in Figure 3b provide a visual indication of device transparency, as well as the uniform illumination at 2 Cd/m$^2$ of a 1 mm $\times$ 2 mm pixel with an applied voltage of 170 $V_{pp}$ at 30 kHz. We test our device using an HP 3254A function generator, which enables us to sweep frequency across a large range with voltages up to 200 $V_{pp}$. We observe that our devices show EL emission at frequencies greater than 10 kHz and with voltages as low as 110 $V_{pp}$ (for operation at 30 kHz). Trends of increasing EL intensity as a function of both increasing voltage and increasing frequency are shown in Figure 3c. While these trends are consistent with impact excitation of the Mn impurity dopant whereby electrons are accelerated across the sputtered ZnS layers, the trends also suggest a possible mechanism in which the high electric field causes an electron to be removed from the valence band of the nanocrystal, leaving a hole behind. An electron from a neighboring nanocrystal, aided by the field, can then couple with the hole to form an exciton on the ZnSe core whose energy can be transferred to the Mn impurity dopant. Further experiments are needed to probe in detail the operating mechanism of these devices.

Figure 3d shows the normalized EL spectra for a device with $Al_2O_3$ (solid orange line) and $HfO_2$ (dashed orange line)

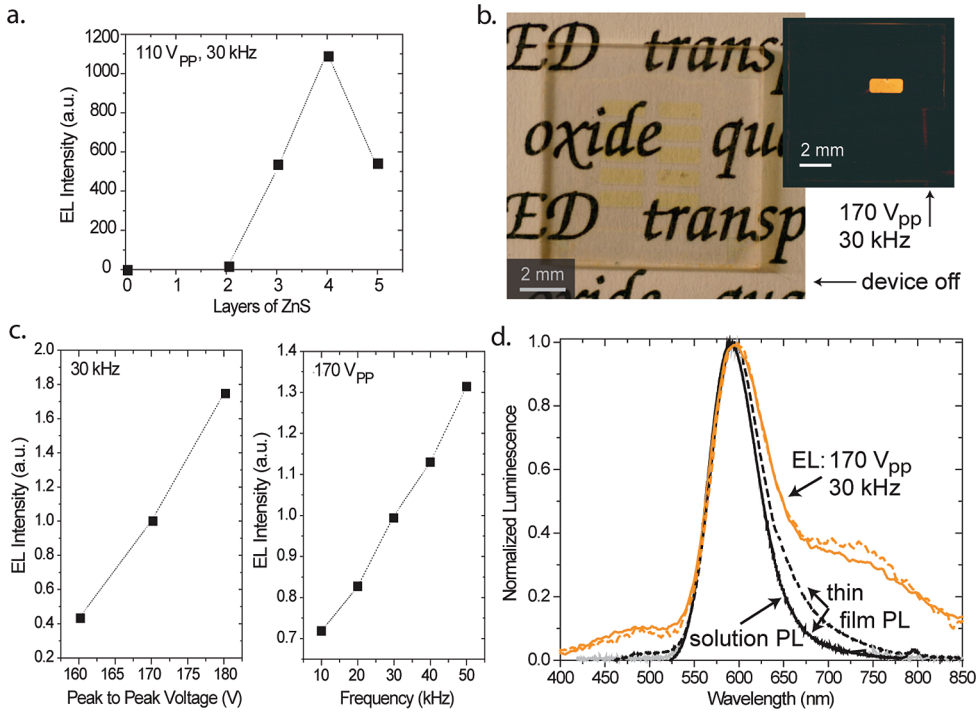


**Figure 3.** (a) Plot of the electroluminescent (EL) intensity versus the number of layers of ZnS in the device structure. We find that for a given bias condition (here, 110 $V_{pp}$ at 30 kHz), devices with four layers of ZnS (and three 30 nm thick layers of nanocrystals) give the largest EL response. (b) A photograph of a 0.5 in. × 0.5 in. glass substrate containing 10 1 mm × 2 mm AC-TFEL devices, with no bias applied. The substrate is pictured on top of printed text to demonstrate the transparency of the AC-TFEL device architecture. The inset shows the uniformity of pixel illumination (in the dark) with the device operating at 170 $V_{pp}$ and 30 kHz. (c) Plots of the EL response as a function of drive voltage and frequency. Values are normalized with respect to the EL response at 170 $V_{pp}$ and 30 kHz. (d) The EL spectra for devices with $Al_2O_3$ and $HfO_2$ insulating layers are presented by the solid and dashed orange curves, respectively. The bias conditions are 170 $V_{pp}$ and 30 kHz. A photoluminescence (PL) spectrum of an incomplete device structure (ITO/$Al_2O_3$/ZnS/30 nm nanocrystals) (solid black curve) matches solution PL spectrum of the nanocrystals in chloroform (solid gray curve). The PL spectrum of a more complete device (consisting of ITO/$Al_2O_3$/ZnS/30 nm nanocrystals/ZnS) in which ZnS has been sputtered onto the nanocrystals is shown with the dashed black line.

insulating layers, both operating at 30 kHz and 170 $V_{pp}$. The overlap of these spectra confirms that the insulating layer does not contribute to or affect the observed EL spectral shape. The dominant peaks in the two EL spectra overlap with the solution PL spectrum (gray line), indicating that the phosphor $^4T_1 \rightarrow {}^6A_1$ transition accounts for the EL response. The broad background emission that spans from 450 nm wavelength into the near-IR is likely a result of electrical excitation of ZnSe defect states that could be created during the sputtered ZnS layer deposition. These defect states could similarly be excited by exciton energy transfer from the ZnSe core. A PL spectrum (black line) of an incomplete device structure (ITO/$Al_2O_3$/ZnS/30 nm nanocrystals) matches the solution PL spectrum and shows no evidence of defect states. However, the PL spectrum of a more complete structure consisting of ITO/$Al_2O_3$/ZnS/30 nm nanocrystals/ZnS (dashed black line) exhibits broadening of the red and blue edges of the nanocrystal luminescence, which is indicative of defect states. The defect states are more prominent in the EL spectra than in the PL spectrum, suggesting that the PL excitation probes all nanocrystals while the EL signal is dominated by nanocrystals at the ZnS interface. While the shape of the EL spectrum is the same regardless of the insulating layer used, the EL intensity is a factor of 2 less for devices using $HfO_2$ instead of $Al_2O_3$. This observation is consistent with a field-driven excitation mechanism for the doped nanocrystals. Since the static dielectric constant of $HfO_2$ is approximately twice that of $Al_2O_3$, we expect that the field drop will be larger across the $HfO_2$ layers than across the $Al_2O_3$ layers in otherwise comparable device structures. This implies a reduction in the electric field across the nanocrystals and ZnS in the $HfO_2$-containing structures, which is consistent with the observed lower EL intensity of $HfO_2$-containing structures.

In summary, we demonstrated ac-driven electroluminescence from highly efficient and stable ZnSe/ZnS:Mn/ZnS nanocrystals. Our device structures contain standard wide band gap ceramic materials which eliminate charge injection into the devices, limiting the electrical excitation of the nanocrystals to field-driven mechanisms. Because the demonstrated device architecture is comparable to existing AC-TFEL technology, our use of spin-casting to deposit the nanocrystals in multilayer stacks highlights the viability of solution-based techniques for depositing the active phosphor layer in AC-TFEL devices, which could enable print fabrication of transparent multicolor AC-TFEL displays.

**Acknowledgment.** The authors thank Dr. Gerry Chen and Dr. Steve Kooi for their assistance. This work is supported by the Institute for Soldier Nanotechnologies (DAAD-19-02-0002), a Presidential Early Career Award for Scientists and Engineers, and a National Defense

Science and Engineering Graduate Fellowship. This work also made use of MRSEC Shared Experimental Facilities at MIT, supported by the National Science Foundation under Award Number DMR-02-13282.

## References

(1) Ono, Y. A. *Electroluminescent Displays*; World Scientific:River Edge, NJ, 1995.
(2) Keir, J. P.; Wager, J. F. *Annu. Rev. Mater. Sci.* **1997**, *27*, 223.
(3) Dur, M.; Goodnick, S. M.; Pennathur, S. S.; Wager, J. F.; Reigrotzki, M.; Redmer, R. *J. Appl. Phys.* **1998**, *83*, 3176.
(4) Li, D.; Clark, B. L.; Keszler, D. A.; Keir, P.; Wager, J. F. *Chem. Mater.* **2000**, *12*, 268.
(5) King, C. *Electroluminescent Displays*; Planar Systems: Beaverton, OR, 2003.
(6) Abileah, A.; Harkonen, K.; Pakkala, A.; Smid, G. *Transparent Electroluminescent (EL) Diplays*, Planar Systems: Beaverton, OR, 2008.
(7) Alivisatos, A. P. *Science* **1996**, *271*, 933.
(8) Shim, M.; Guyot-Sionnest, P. *Nature* **2000**, *407*, 981.
(9) Levy, L.; Hochepied, J. F.; Pileni, M. P. *J. Phys. Chem.* **1996**, *100*, 18322.
(10) Hanif, K. M.; Meulenberg, R. W.; Strouse, G. F. *J. Am. Chem. Soc.* **2002**, *122*, 2532.
(11) Wang, Y.; Herron, N.; Moller, K.; Bein, T. *Solid State Commun.* **1991**, *77*, 33.
(12) Norris, D. J.; Yao, N.; Charnock, F. T.; Kennedy, T. A. *Nano Lett.* **2007**, *1*, 3.
(13) Pradhan, N.; Goorskey, D.; Thessing, J.; Peng, X. *J. Am. Chem. Soc.* **2005**, *127*, 17528.
(14) Pradhan, N.; Peng, X. *J. Am. Chem. Soc.* **2006**, *129*, 3339.
(15) Yang, H.; Santra, S.; Holloway, P. H. *J. Nanosci. Nanotechnol.* **2005**, *5*, 1364.
(16) Coe, S.; Woo, W.; Bawendi, M. G.; Bulović, V. *Nature* **2002**, *420*, 800.
(17) Caruge, J.-M.; Halpert, J. E.; Wood, V.; Bawendi, M. G.; Bulović, V. *Nat. Photonics* **2008**, *2*, 247.
(18) Kim, L. A.; Anikeeva, P. O.; Coe-Sullivan, S. A.; Steckel, J. S.; Bawendi, M. G.; Bulović, V. *Nano Lett.* **2008**, *8*, 4513.
(19) Wood, V.; Panzer, M. J.; Chen, J. L.; Bradley, M. S.; Halpert, J. E.; Bawendi, M. G.; Bulović, V. *Adv. Mater.* **2009**, *21*, published online March 4.
(20) Kobayashi, S.; Tani, Y.; Kawazoe, H. *Jpn. J. Appl. Phys.* **2007**, *46*, L966.
(21) Thakar, R.; Chen, Y.; Snee, P. T. *Nano Lett.* **2007**, *7*, 3429.

NL900898T